Field-induced multiple quantum phase transitions in the antiferromagnetic Kondo-lattice compound $CeRhAl_4Si_2$

Honghong Wang,[1,*] Tae Beom Park,[1,2,*] Soohyeon Shin,[1,3] Harim Jang,[1] Eric D. Bauer,[4] and Tuson Park[1,†]

[1]*Center for Quantum Materials and Superconductivity (CQMS) and Department of Physics, Sungkyunkwan University, Suwon 16419, South Korea*

[2]*Institute of Basic Science, Sungkyunkwan University, Suwon 16419, South Korea*

[3]*Laboratory for Multiscale Materials Experiments, Paul Scherrer Institut, CH-5232 Villigen PSI, Switzerland*

[4]*Los Alamos National Laboratory - Los Alamos, New Mexico 87545, USA*

(Received 11 February 2022; revised 24 March 2022; accepted 25 March 2022; published 7 April 2022)

We report a comprehensive phase diagram of the antiferromagnetic Kondo-lattice compound $CeRhAl_4Si_2$ down to 0.3 K by investigating electrical resistivity, magnetoresistivity, and Hall resistivity under the magnetic field along the c axis. At zero field, $CeRhAl_4Si_2$ undergoes two successive antiferromagnetic transitions at $T_{N1} = 14.2$ K and $T_{N2} = 8.4$ K, respectively. Upon applying magnetic field, the first-order transition of T_{N2} is continuously suppressed at the critical field of 5.5 T. On the other hand, the smooth suppression of the second-order transition of T_{N1} terminates at a tricritical point of 6.6 T and 4.7 K, followed by a first-order transition line and an additional phase transition line, which are monotonically suppressed at 6.7 and 7.2 T, respectively, implying the field-induced multiple quantum phase transitions. Particularly, in the paramagnetic region before the Fermi liquid behavior is fully developed, a quantum critical phase with non-Fermi liquid behavior is revealed, indicating a potential spin liquid state that was predicted from the global quantum phase diagram. These results suggest that $CeRhAl_4Si_2$ is a promising candidate to study a quantum phase transition that occurs in electronic systems with high degree of frustration.

DOI: 10.1103/PhysRevB.105.165110

The physics of quantum criticality has been one of the foremost challenges in strongly correlated electron systems, which is regarded as a key to understanding the important issues including the nature of unconventional superconductivity and non-Fermi liquid (nFL) behavior [1,2]. In contrast to the classical phase transition driven by thermal fluctuations, the quantum phase transition (QPT) is triggered by quantum fluctuations at zero temperature via nonthermal parameters such as pressure, chemical substitution, or magnetic field [3]. Heavy-fermion (HF) compounds are prototype systems to study the QPT owing to the delicate competition between the Kondo effect and the Ruderman-Kittel-Kasuya-Yosida interaction that promote a nonmagnetic and magnetic ground state, respectively. Various types of quantum criticality, including the Kondo breakdown type [4] and the spin-density-wave type [5], have been revealed in HF systems [6–8]. Therefore, it is instructive to broaden the materials basis to establish a universal understanding of the rich variety of quantum critical points (QCPs).

$CeT_mAl_{2m+2}Si_2$ (T = Rh, Ir, Pt) is a family of HF systems, which crystallizes in a tetragonal structure (space group $P4/mmm$) and is composed of two alternate stacking of a Ce-containing $BaAl_4$-type layer and a T-containing $AuAl_2$-type block along the c axis [9,10]. The systematically tunable dimensionality has attracted attention to this family, which could provide the key to controlling the nature of QCP [11,12] and the superconducting transition temperature [13]. However, the quantum criticality in this $CeT_mAl_{2m+2}Si_2$ series has yet to be fully unveiled due to the insufficient study at low temperatures.

$CeRhAl_4Si_2$, which belongs to the class with $m = 1$, is an antiferromagnetic (AFM) HF compound that undergoes two successive AFM transitions of $T_{N1} = 14.2$ K and $T_{N2} = 8.4$ K at 0 T [9,10], where T_{N2} is the magnetic transition from an incommensurate with $\mathbf{k}_{IC} = (0.016, 0.016, 1/2)$ to a commensurate structure with $\mathbf{k}_C = (0, 0, 1/2)$ [14–16]. When subjected to a magnetic field, these two AFM transitions are suppressed [10], implying a potential field-induced QCP in this compound. To investigate the quantum criticality, we carried out the measurements at low temperatures, particularly at temperatures below 1.8 K, which have not been performed in the previous report [10]. Here, we present in-plane low-temperature transport measurements down to 0.3 K on $CeRhAl_4Si_2$ with the applied field along the c axis. Our results demonstrate that, under field, the lower AFM transition T_{N2} retains first-order character, while the higher AFM transition T_{N1} changes its nature from second to first order accompanied by the appearance of another phase. With further increasing field, the first-order transition and the other phase are suppressed at 6.7 and 7.2 T, respectively, indicating field-induced multiple quantum phase transitions. Furthermore, evidence for the nFL behavior is observed in the intermediate phase between the ordered phase and the Fermi liquid (FL) region, suggesting a possible field-induced spin liquid state [17].

*These authors have contributed equally to this work.

†Corresponding author: tp8701@skku.edu

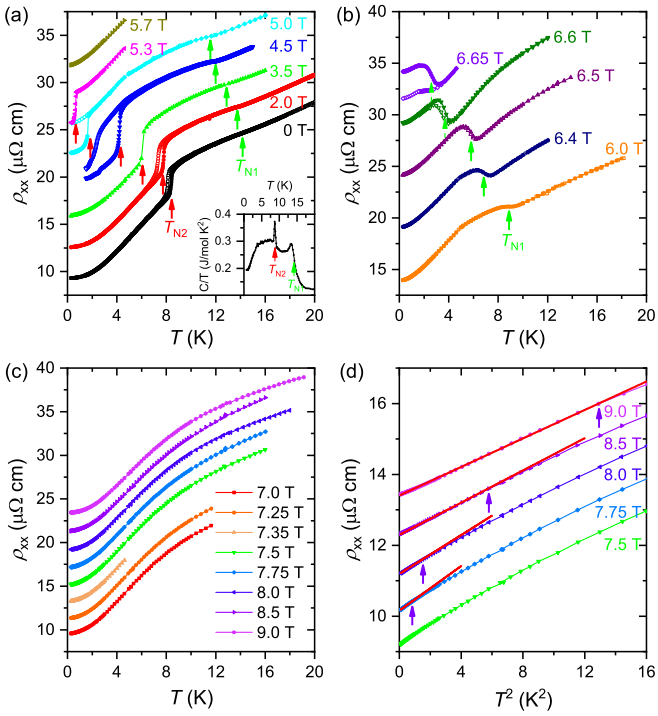

FIG. 1. (a)–(c) Temperature dependence of in-plane resistivity $\rho_{xx}(T)$ for $CeRhAl_4Si_2$ at various fields applied along the c axis. T_{N1} (green arrows) and T_{N2} (red arrows) correspond to the higher second-order and the lower first-order AFM transition temperatures, respectively. After the higher second-order AFM transition changes to a first-order transition above 6.6 T, T_{N1} is marked by the dashed green arrows. Solid symbols represent data measured with increasing temperature and zero-field-cooling mode. Open symbols represent data measured with decreasing temperature and field-cooling mode. The first-order nature of transition is revealed by the hysteretic behavior. Inset of (a) shows the temperature dependence of specific heat divided by temperature C/T at 0 T. (d) Low-temperature resistivity is plotted as a function of T^2 for fields above 7.5 T. Violet arrows mark the Fermi liquid temperature below which $\rho_{xx}(T)$ follows T^2 dependence. The solid red lines are least-squares fits to $\rho_{xx}(T) = \rho_0 + AT^2$. For clarity, resistivity data at different fields have been shifted vertically by 3, 5, 2, and 1 $\mu\Omega$ cm in (a)–(d), respectively.

Single crystals of $CeRhAl_4Si_2$ were synthesized using the Al/Si flux method as described earlier [9]. All the measurements were performed using the standard six-probe alternating current technique on a rectangular platelet with dimensions of $0.94 \times 0.32 \times 0.05\,\text{mm}^3$, with the current flowing within the ab plane and the applied magnetic field parallel to the c axis. The low-resistance contacts were obtained by spot welding 25-μm-diameter Pt wires onto the sample. Magnetoresistivity and Hall resistivity were measured simultaneously by conducting isothermal field sweeps and accurately determined by reversing the magnetic field. The specific heat was carried out using a homemade calorimetry setup employing a thermal relaxation method. A ^{3}He refrigerator was used to control temperature down to 0.3 K and magnetic field up to 9 T.

Figure 1 shows the temperature dependence of the in-plane resistivity $\rho_{xx}(T)$ for $CeRhAl_4Si_2$ under various magnetic fields applied along the c axis ($B||c$). At zero field, two AFM transitions are detected in the low-temperature measurements, which is consistent with the previous reports [9,10]. The lower AFM transition at $T_{N2} = 8.4$ K appears as an abrupt jump in the resistivity and a sharp peak in the specific heat. On the other hand, for the higher AFM transition at $T_{N1} = 14.2$ K, there is a relatively weak slope change in the resistivity, which can be discernible from the first derivative of resistivity (not shown) and the clear cusp feature in the specific heat as shown in the inset of Fig. 1(a). The hysteresis behavior of the resistivity and the shape of the sharp peak in the specific heat support that the transition at T_{N2} is of a first-order nature. With applying field, T_{N2} shifts toward lower temperatures and is completely suppressed below 0.3 K at 5.7 T [Fig. 1(a)]. The hysteresis behavior becomes clearer under field, indicating that T_{N2} retains the nature of a first-order transition. Accompanied by the suppression of T_{N1}, the signature corresponding to T_{N1} becomes more visible with increasing field, which appears as a clear kink and then becomes an upturn in $\rho_{xx}(T)$ [Figs. 1(a) and 1(b)]. As the field further increases to 6.6 T, hysteresis appears near the upturn, which exceeds the experimental error and is enhanced with an increase in the field, indicating that the character of T_{N1} changes from second to first order. This first-order transition is further suppressed by increasing magnetic field and becomes unresolvable above 7.0 T [Fig. 1(c)]. With further increasing field, a T^2 dependence is observed at fields higher than 7.5 T, as shown in Fig. 1(d), implying the recovery of FL behavior.

To confirm the evolution of the two AFM transitions with the field observed in $\rho_{xx}(T)$, the field-dependent magnetoresistivity $\rho_{xx}(B)$ was performed in the transverse geometry with the field applied parallel to the c axis and the current within the ab plane at selected temperatures. The isothermal $\rho_{xx}(B)$ at 0.3 K with increasing (solid symbols) and decreasing (open symbols) field sweeps is presented in Fig. 2(a). Analogous to the profiles observed in $CeAuSb_2$ [18], YbAgGe [19], CePdAl [20], and $CePtIn_4$ [21], $\rho_{xx}(B)$ initially increases with field (which is a typical characteristic of AFM order), jumps sharply through the first metamagnetic transition (MMT) at B_1, is almost flat, and then decreases sharply across the second MMT at B_2. It is noteworthy that $\rho_{xx}(B)$ shows a clear hysteresis at two MMTs in the field return cycle. The first-order nature of these transitions is consistent with the hysteresis observed in the $\rho_{xx}(T)$ measurements. At higher fields, a shoulder appearing at B_3 is indicative of another field-induced phase transition. With further increasing field, a local minimum of $\rho_{xx}(B)$ occurs at B_4, which can be ascribed to the competition between the positive contribution from the cyclotron motion of the conduction electrons and the negative contribution from the suppression of spin fluctuations by the applied field [10,21]. Above B_4, the contribution associated with the cyclotron motion of electrons dominates and the positive slope is observed as in the normal metals. The sequence of the multiple transitions can be unambiguously deduced from the first derivative of $\rho_{xx}(B)$, as shown in Fig. 2(b).

Figure 2(c) displays the isothermal Hall resistivity $\rho_{xy}(B)$ at 0.3 K, which was carried out simultaneously with $\rho_{xx}(B)$ to explore the possible changes in the electronic structure across the critical fields. Similar to the features in the $\rho_{xx}(B)$, each transition can be identified in $\rho_{xy}(B)$ as well. The sudden changes in $\rho_{xy}(B)$ appear when the field crosses the two

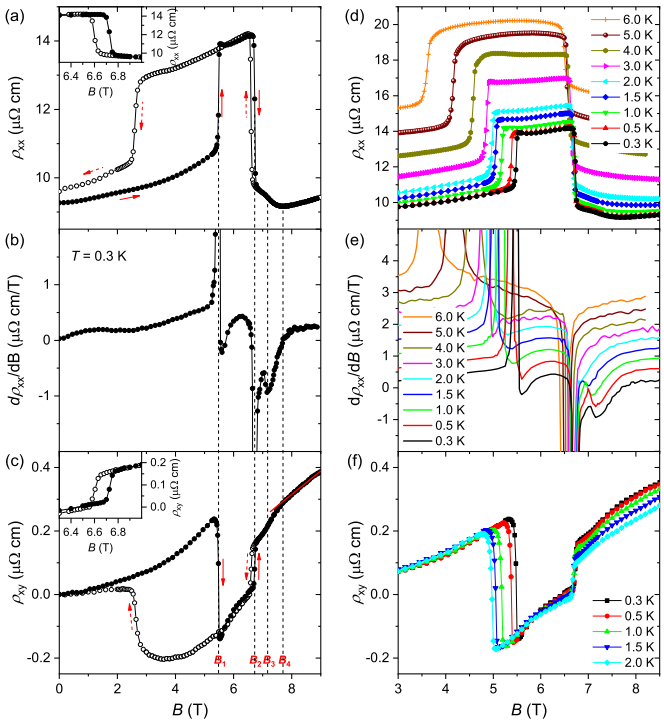

FIG. 2. Isotherms of magnetoresistivity $\rho_{xx}(B)$, differential magnetoresistivity $d\rho_{xx}(B)/dB$, and Hall resistivity $\rho_{xy}(B)$ for $CeRhAl_4Si_2$ measured at $T = 0.3$ K (a)–(c) and at representative temperatures between $T = 0.3$ and 6.0 K (d)–(f). A clear hysteresis is visible in the field-up and -down cycle in (a) and (c), illustrating the first-order nature of the two MMTs at lower temperatures. Solid and dashed arrows indicate field-up and -down sweeps, respectively. Dashed lines in (a)–(c) indicate the critical fields marked by B_1, B_2, B_3, and B_4, corresponding to the sequence of transitions. The insets in (a) and (c) are enlarged views of the hysteresis near the MMT at B_2. Red line in (c) is the linear fit to $\rho_{xy}(B)$. For clarity, $d\rho_{xx}(B)/dB$ in (e) has been shifted vertically by 0.4 $\mu\Omega$ cm/T.

MMTs at B_1 and B_2, which can be related to the reconstruction of the Fermi surface [22–24]. As the field is further increased, a clear kink is observed at B_3. For field higher than B_4, $\rho_{xy}(B)$ shows a linear field dependence (red line), suggesting the formation of the FL state, which is coincident with the recovery of the positive slope in $\rho_{xx}(B)$. Similar field dependence is also observed in YbAgGe at the critical field above which FL state is formed [25]. Figures 2(d)–2(f) show representative field-dependent $\rho_{xx}(B)$, $d\rho_{xx}(B)/dB$, and $\rho_{xy}(B)$, respectively, at various temperatures below 6 K. As the temperature increases, the changes at the two MMTs remain sharp and shift to lower fields, while the feature for the third phase gradually weakens and cannot be discerned at temperatures above 2 K.

In accordance with $\rho_{xx}(B)$ and $\rho_{xy}(B)$, the phase boundaries can be established by the specific heat (C) measurements. Figure 3 shows the field dependence of specific heat at 0.3 K, plotted as $C(B)/T$. It clearly reveals a sudden jump across B_1 and reaches a pronounced maximum at B_2, corresponding to the two metamagnetic transitions. Moreover, the appearance of a broad kink at B_3 is consistent with the formation of another field-induced phase. The enhancement of C/T is suggestive of the magnetic fluctuations associated with the underlying QCP.

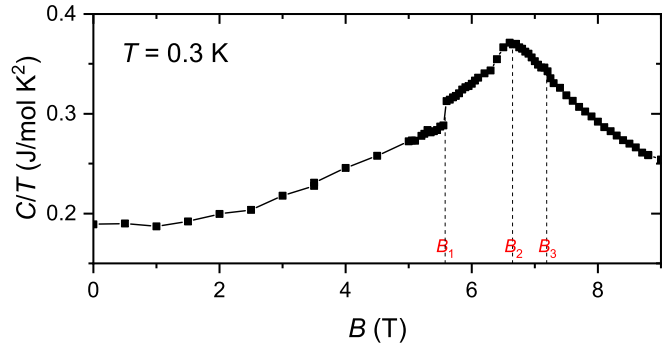

FIG. 3. Field dependence of specific heat divided by temperature C/T for $CeRhAl_4Si_2$ measured at 0.3 K. Dashed lines indicate the critical fields marked by B_1, B_2, and B_3, corresponding to the critical fields as shown in Fig. 2.

The results obtained from the above experimental measurements are summarized in the temperature-field (T-B) phase diagram in Fig. 4 (see also Supplemental Material [26] for another comprehensive T-B phase diagram that shows hysteretic regions.). The lower AFM phase, marked as AFM2, is fully suppressed at the critical field $B_{c1} = 5.5$ T and its first-order nature is clearly evidenced by the large hysteresis behavior in $\rho_{xx}(T)$, $\rho_{xx}(B)$, and $\rho_{xy}(B)$. However, the smooth suppression of the higher AFM phase, denoted as AFM1, is terminated by the change from a second- to first-order transition at about 6.6 T and 4.7 K, which is manifested by the appearance of the moderate hysteresis in $\rho_{xx}(T)$, $\rho_{xx}(B)$, and $\rho_{xy}(B)$. This first-order transition is suppressed at the critical field $B_{c2} = 6.7$ T. The vertical phase-boundary line at B_{c2} indicates that the field-induced QCP observed in $YbRh_2Si_2$ [27] is avoided. In addition, another phase, represented by M, starts to appear at the critical field $B_{c3} = 7.2$ T and increases with a decrease in the field. The appearance of M phase is reminiscent of the d phase in YbAgGe [28,29]. Considering the similarities between the phase diagram in these two compounds, it can be conjectured that there is a putative tricritical point at about 6.6 T and 4.7 K where the M phase emerges and the AFM1 phase becomes a first-order transition. The M phase of $CeRhAl_4Si_2$ in magnetic field may correspond to a different magnetic state with a different ordering wave vector. Further measurements of the magnetic structure with $B||c$ are necessary to clarify the nature of the M phase.

In addition to the complexity of field-induced multiple quantum phase transitions, the characteristic of the paramagnetic (PM) phase is also intriguing. The power-law analysis of $\rho_{xx}(T)$, $\rho_{xx}(T) = \rho_0 + AT^n$, was carried out above 7 T. As shown in the inset of Fig. 4, n is initially smaller than 2 in the PM phase and gradually increases to 2 at $B_{c4} = 7.7$ T, signaling that the FL state is recovered in the high-field regime. The critical field B_{c4} is in agreement with the recovery of the positive slope in $\rho_{xx}(B)$ and the linear-field dependence of $\rho_{xy}(B)$ (Fig. 2). These discoveries indicate that, preceding the development of the FL state, there is an intermediate phase ($B_{c3} < B < B_{c4}$) within which $\rho_{xx}(T)$ exhibits nFL behavior. We note that similar quantum critical phase has been reported in other HF systems, such as YbAgGe [19,29], CePdAl [30,31], Ir-substituted $YbRh_2Si_2$ [32], and Ge-substituted

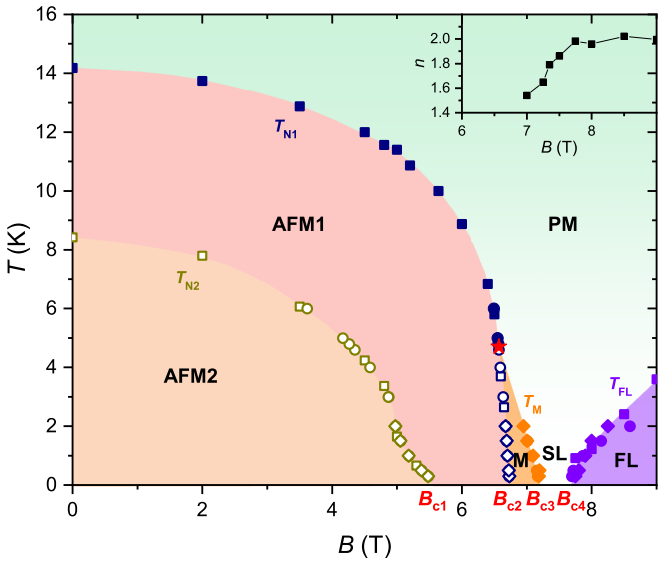

FIG. 4. Temperature-field (T-B) phase diagram of $CeRhAl_4Si_2$ for field applied along the c axis. The dark yellow squares, circles, and diamonds denote the lower first-order AFM transition at T_{N2} determined by resistivity $\rho_{xx}(T)$, magnetoresistivity $\rho_{xx}(B)$, and Hall resistivity $\rho_{xy}(B)$ measurements, respectively. The solid navy squares and circles represent the higher second-order AFM transition at T_{N1} determined by $\rho_{xx}(T)$ and $\rho_{xx}(B)$ measurements, respectively. The open navy squares, circles, and diamonds denote the first-order AFM transition at T_{N1} obtained by $\rho_{xx}(T)$, $\rho_{xx}(B)$, and $\rho_{xy}(B)$ measurements, respectively. The orange circles and diamonds mark the characteristic temperature T_M for the field-induced phase deduced from $\rho_{xx}(B)$ and $\rho_{xy}(B)$ measurements, respectively. The violet circles and diamonds identify the critical fields where the slope of $\rho_{xx}(B)$ recovers to be positive and $\rho_{xy}(B)$ shows linear B dependence. The violet squares are the onset of the T^2-dependent resistivity behavior. B_{c1}, B_{c2}, B_{c3}, and B_{c4} correspond to the phase boundaries separating the two antiferromagnetic phases (AFM1 and AFM2), the field-induced phase (M), the intermediate quantum critical phase (SL), and the Fermi liquid phase (FL). The red star indicates the possible tricritical point. All the first-order phase transition points (open symbols) were taken from either increasing-magnetic field or increasing-temperature measurements with zero-field-cooling mode. Inset shows the field dependence of exponent n resulting from the power-law fits to the $\rho_{xx}(T)$ data of the form $\rho_{xx}(T) = \rho_0 + AT^n$. PM represents the paramagnetic phase.

$YbRh_2Si_2$ [33]. The global phase diagram for HF metals [17], which is spanned by two parameters of the Kondo coupling (J_K) and the magnetic frustration or the spatial dimensionality (G), provides a possible explanation for the quantum critical phase. With the application of field, the $CeRhAl_4Si_2$ system may follow a trajectory that goes through a spin liquid state when it evolves from the magnetic ordered phase to the PM phase. More measurements at even lower temperatures, especially that are sensitive to the low-energy spin excitations, would be desirable to understand the quantum spin liquid state. In addition, in the $CeT_mAl_{2m+2}Si_2$ family, the thickness of the TAl_2 block can be enlarged by increasing m, thus resulting in the increase of the distance between the adjacent Ce planes. The decrease of the effective dimensionality, consequently, is expected to increase the degree of frustration G, placing $CeT_mAl_{2m+2}Si_2$ with larger m value in the upper part of the global phase diagram. These results suggest that $CeT_mAl_{2m+2}Si_2$ is a promising platform for the exploration of a novel quantum spin liquid phase in vicinity of the quantum criticality.

In conclusion, we performed electrical resistivity, magnetoresistivity, specific heat, and Hall resistivity measurements on $CeRhAl_4Si_2$ and constructed a comprehensive T-B phase diagram down to 0.3 K with the field applied along the c axis. The two successive AFM transitions decrease with increasing field. The first-order AFM transition at T_{N2} is continuously suppressed at 5.5 T while the suppression of the second-order AFM transition at T_{N1} is terminated at a tricritical point 6.6 T and 4.7 K, where it is bifurcated into the first-order AFM transition line and the other phase transition line. Further experimental work such as neutron scattering on $CeRhAl_4Si_2$ with field applied along the c axis will be important to understand the nature of the field-induced multiple quantum phase transitions, especially the intermediate phase that may arise from novel quantum spin liquids.

This work was supported by the National Research Foundation (NRF) of Korea through a grant funded by the Korean Ministry of Science and ICT (Grants No. 2021R1A2C2010925 and No. 2021R1I1A1A01047499). Work at Los Alamos was performed under the auspices of the U.S. Department of Energy, Office of Basic Energy Sciences, Division of Materials Science and Engineering.

[1] T. Moriya and K. Ueda, Rep. Prog. Phys. **66**, 1299 (2003).
[2] H. v. Löhneysen, A. Rosch, M. Vojta, and P. Wölfle, Rev. Mod. Phys. **79**, 1015 (2007).
[3] S. Sachdev, *Quantum Phase Transitions* (Cambridge University Press, Cambridge, UK, 2001).
[4] Q. Si, S. Rabello, K. Ingersent, and J. L. Smith, Nature (London) **413**, 804 (2001).
[5] A. J. Millis, Phys. Rev. B **48**, 7183 (1993).
[6] P. Gegenwart, Q. Si, and F. Steglich, Nat. Phys. **4**, 186 (2008).
[7] Q. Si and F. Steglich, Science **329**, 1161 (2010).
[8] S. Paschen and Q. Si, Nat. Rev. Phys. **3**, 9 (2021).
[9] N. J. Ghimire, F. Ronning, D. J. Williams, B. L. Scott, Y. Luo, J. D. Thompson, and E. D. Bauer, J. Phys.: Condens. Matter **27**, 025601 (2015).
[10] A. Maurya, R. Kulkarni, A. Thamizhavel, D. Paudyal, and S. K. Dhar, J. Phys. Soc. Jpn. **85**, 034720 (2016).
[11] P. Coleman and A. H. Nevidomskyy, J. Low Temp. Phys. **161**, 182 (2010).
[12] Q. Si, J. H. Pixley, E. Nica, S. J. Yamamoto, P. Goswami, R. Yu, and S. Kirchner, J. Phys. Soc. Jpn. **83**, 061005 (2014).
[13] P. Monthoux and G. G. Lonzarich, Phys. Rev. B **69**, 064517 (2004).
[14] N. J. Ghimire, S. Calder, M. Janoschek, and E. D. Bauer, J. Phys.: Condens. Matter **27**, 245603 (2015).
[15] H. Sakai, T. Hattori, Y. Tokunaga, S. Kambe, N. J. Ghimire, F. Ronning, E. D. Bauer, and J. D. Thompson, Phys. Rev. B **93**, 014402 (2016).

[16] J. Gunasekera, L. Harriger, A. Dahal, A. Maurya, T. Heitmann, S. M. Disseler, A. Thamizhavel, S. Dhar, D. J. Singh, and D. K. Singh, Phys. Rev. B **93**, 155151 (2016).
[17] Q. Si, Phys. Status Solidi B **247**, 476 (2010).
[18] L. Balicas, S. Nakatsuji, H. Lee, P. Schlottmann, T. P. Murphy, and Z. Fisk, Phys. Rev. B **72**, 064422 (2005).
[19] P. G. Niklowitz, G. Knebel, J. Flouquet, S. L. Bud'ko, and P. C. Canfield, Phys. Rev. B **73**, 125101 (2006).
[20] H. Zhao, J. Zhang, S. Hu, Y. Isikawa, J. Luo, F. Steglich, and P. Sun, Phys. Rev. B **94**, 235131 (2016).
[21] D. Das, D. Gnida, P. Wiśniewski, and D. Kaczorowski, Proc. Natl. Acad. Sci. **116**, 20333 (2019).
[22] R. Daou, C. Bergemann, and S. R. Julian, Phys. Rev. Lett. **96**, 026401 (2006).
[23] S. M. Thomas, P. F. S. Rosa, S. B. Lee, S. A. Parameswaran, Z. Fisk, and J. Xia, Phys. Rev. B **93**, 075149 (2016).
[24] G. G. Marcus, D.-J. Kim, J. A. Tutmaher, J. A. Rodriguez-Rivera, J. O. Birk, C. Niedermeyer, H. Lee, Z. Fisk, and C. L. Broholm, Phys. Rev. Lett. **120**, 097201 (2018).
[25] S. L. Bud'ko, V. Zapf, E. Morosan, and P. C. Canfield, Phys. Rev. B **72**, 172413 (2005).
[26] See Supplemental Material at http://link.aps.org/supplemental/10.1103/PhysRevB.105.165110 for a complete set of isotherms of magnetoresistivity measured at representative temperatures in a field up and down cycle and another comprehensive *T-B* phase diagram that shows hysteretic regions.
[27] J. Custers, P. Gegenwart, H. Wilhelm, K. Neumaier, Y. Tokiwa, O. Trovarelli, C. Geibel, F. Steglich, C. Pépin, and P. Coleman, Nature (London) **424**, 524 (2003).
[28] E. Mun, S. L. Bud'ko, and P. C. Canfield, Phys. Rev. B **82**, 174403 (2010).
[29] G. M. Schmiedeshoff, E. D. Mun, A. W. Lounsbury, S. J. Tracy, E. C. Palm, S. T. Hannahs, J. H. Park, T. P. Murphy, S. L. Bud'ko, and P. C. Canfield, Phys. Rev. B **83**, 180408(R) (2011).
[30] H. Zhao, J. Zhang, M. Lyu, S. Bachus, Y. Tokiwa, P. Gegenwart, S. Zhang, J. Cheng, Y.-f. Yang, G. Chen, Y. Isikawa, Q. Si, F. Steglich, and P. Sun, Nat. Phys. **15**, 1261 (2019).
[31] J. Zhang, H. Zhao, M. Lv, S. Hu, Y. Isikawa, Y.-f. Yang, Q. Si, F. Steglich, and P. Sun, Phys. Rev. B **97**, 235117 (2018).
[32] S. Friedemann, T. Westerkamp, M. Brando, N. Oeschler, S. Wirth, P. Gegenwart, C. Krellner, C. Geibel, and F. Steglich, Nat. Phys. **5**, 465 (2009).
[33] J. Custers, P. Gegenwart, C. Geibel, F. Steglich, P. Coleman, and S. Paschen, Phys. Rev. Lett. **104**, 186402 (2010).